Monthly Notices
of the
ROYAL ASTRONOMICAL SOCIETY

MNRAS **468,** 418–425 (2017)
Advance Access publication 2017 February 24

doi:10.1093/mnras/stx480

The mass distribution of Population III stars

M. Fraser,[1,2⋆] A. R. Casey,[2] G. Gilmore,[2] A. Heger[3,4,5] and C. Chan[3]

[1]*School of Physics, O'Brien Centre for Science North, University College Dublin, Belfield, Dublin 4, Ireland*
[2]*Institute of Astronomy, University of Cambridge, Madingley Road, Cambridge CB3 0HA, UK*
[3]*Monash Centre for Astrophysics, School of Physics and Astronomy, Monash University, 19 Rainforest Walk, Vic 3800, Australia*
[4]*Department of Physics and Astronomy, Shanghai Jiao-Tong University, CNA, Shanghai 200240, P. R. China*
[5]*School of Physics and Astronomy, University of Minnesota, Minneapolis, MN 55455, USA*

Accepted 2017 February 22. Received 2017 February 22; in original form 2015 November 8

ABSTRACT

Extremely metal-poor (EMP) stars are uniquely informative on the nature of massive Population III stars. Modulo a few elements that vary with stellar evolution, the present-day photospheric abundances observed in EMP stars are representative of their natal gas cloud composition. For this reason, the chemistry of EMP stars closely reflects the nucleosynthetic yields of supernovae from massive Population III stars. Here we collate detailed abundances of 53 EMP stars from the literature and infer the masses of their Population III progenitors. We fit a simple initial mass function (IMF) to a subset of 29 of the inferred Population III star masses, and find that the mass distribution is well represented by a power-law IMF with exponent $\alpha = 2.35^{+0.29}_{-0.24}$. The inferred maximum progenitor mass for supernovae from massive Population III stars is $M_{\rm max} = 87^{+13}_{-33}$ M$_\odot$, and we find no evidence in our sample for a contribution from stars with masses above ∼120 M$_\odot$. The minimum mass is strongly consistent with the theoretical lower mass limit for Population III supernovae. We conclude that the IMF for massive Population III stars is consistent with the IMF of present-day massive stars and there may well have formed stars much below the supernova mass limit that could have survived to the present day.

Key words: stars: abundances – stars: formation – stars: Population III – supernovae: general.

1 INTRODUCTION

Population III stars formed from primordial metal-free gas, and can be subdivided into Population III.1 and III.2 stars. The former are completely unaffected by preceding star formation, while the latter may have been effected by energy input from previous star formation, but not chemically enriched (O'Shea et al. 2008). Of these stars, only those which had masses below $\lesssim$0.8 M$_\odot$ could have survived to the present day. No low-mass Population III star has been discovered thus far, however, despite decades of intensive searching (e.g. Beers & Christlieb 2005; Christlieb et al. 2008; Norris et al. 2013; Jacobson et al. 2015; Schlaufman & Casey 2014). The absence of an unambiguous detection of a low-mass Population III star means that both the individual and ensemble properties of these stars remain unknown. The initial mass function (IMF) which governs the relative frequency of stars as a function of mass, appears to be fairly uniform today (Bastian, Covey & Meyer 2010). In the early Universe, however, the conditions for star formation were presumably quite different, and there have been long theoretical arguments that many more extremely massive (∼10^2–10^{3}M$_\odot$) stars would have formed (e.g. Bromm, Coppi & Larson 1999). More recently, this has been questioned, with increased spatial resolution in simulations of metal-free star formation and an improved understanding of the role of cooling from molecular hydrogen. This work suggests that fragmentation occurs, and that lower mass metal-free stars can be produced (e.g. Clark et al. 2011; Greif et al. 2011).

To determine the IMF for Population III stars, we need to count the number of massive stars in the early Universe. Because we cannot observe individual members of the first generation of massive stars in the foreseeable future, we are forced to turn to indirect tracers. One such probe is spectroscopy of galaxies, which can reveal the signature of a large number of Population III stars (Schaerer 2002; Sobral et al. 2015). Alternatively, one can search for the explosion of Population III stars as high-redshift supernovae (Whalen et al. 2013). Finally, it is also possible to study Population III stars through their chemical imprint on subsequent generations of low-mass stars (Heger & Woosley 2002, 2010).

Extremely metal-poor (EMP) stars are thought to have formed out of material that has been enriched by very few (or just one) supernovae. While they will burn H to form He, low-mass stars will not produce any heavy elements in their cores, and hence the abundances measured in EMP stars from high-resolution spectra generally reflect the composition of the gas from which that star

⋆ E-mail: morgan.fraser@ucd.ie

formed. If this gas has been polluted by only a single supernova, then these same abundances provide information on its progenitor and explosion parameters. Through comparison to models of supernova nucleosynthesis, we can infer both the mass of the progenitor and the supernova explosion energy (Tominaga, Iwamoto & Nomoto 2014; Placco et al. 2015; Ji, Frebel & Bromm 2015). One important exception to this is the case of giant stars, which have evolved off the main sequence. For these stars, dredge-up can mix CNO processed material from the core of the star to the surface, altering the abundances in these elements. For this reason, we consider the combined CNO abundances in these objects (Section 3).

In this Letter we assemble a large sample of EMP stars from the literature, and use them to determine the mass range of massive Population III stars and infer the slope of the IMF. We also consider whether there is any evidence for pair-instability supernovae based on the chemical abundances of stars in the Milky Way. In Sections 2 and 3 we outline our literature sample of observational data, the methodology for determining the mass of the progenitors of Population III SNe, and the procedure for fitting the IMF. In Section 4 we discuss our results and draw conclusions.

2 DATA

We searched the literature for EMP stars with detailed chemical abundances. For stars with progressively higher metallicities, there is a greater likelihood that the star has been polluted by multiple generations of previous supernovae. Indeed, given the right combination of progenitor mass and explosion energy, a single primordial supernova can enrich some of the interstellar medium to a level of [Fe/H] ~ -3 (e.g. Chen et al. 2015). For these reasons we place an arbitrary cut of [Fe/H] < -3.5 on our sample. This threshold provides us with a sufficient number of metal-poor stars with detailed chemical information ($\sim$50), but limits the number of stars that are more likely to have formed from multiple supernovae.

We first queried the SAGA data base[1] to create a catalogue of stars with metallicities [Fe/H] < -3.5. We complemented this search with recently published works from the literature. We sourced measured abundances directly from the original literature (i.e. not from heterogeneous compilations like this work) and converted the published abundance quantities (typically [X/H] or [X/Fe]) to $\log_\epsilon$(X) values using the solar abundance scale quoted in each paper. For stars with chemical abundances published in multiple papers, we favoured more recent literature sources. The complete sample of metal-poor stars used in this work, along with their stellar parameters and the references to the original literature are listed in Table 1.

In several cases there were more than one set of chemical abundances quoted for a single star. In these scenarios we opted for the most 'representative' chemical abundances. Specifically we opted for chemical abundances measured using $\langle$3D$\rangle$ model photospheres, abundances adjusted using trustworthy non-local thermodynamic equilibrium (LTE) corrections, or abundances measured from ionized species (over neutral species) wherever possible. These choices were adopted to minimize systematic effects (e.g. non-LTE departures), which can be significant in EMP stars.

Our literature search revealed many low-metallicity stars with abundance measurements for just a few elements. These stars were faint (some with $V \sim 20$), and therefore require a significant 8 m class telescope time investment merely to confirm their metal-poor nature. Low signal-to-noise ratio (S/N) and/or limited wavelength coverage further precluded any detailed chemical analysis of these stars. This point highlights the need for apparently bright EMP stars, where the detailed chemistry can be inferred using existing telescope/instrument combinations (e.g. Schlaufman & Casey 2014; Casey & Schlaufman 2015). Previous studies (e.g. Bessell et al. 2015) have commented on the necessity of C, N, and other light-element abundances in order to accurately infer supernova progenitor masses. For these reasons, literature stars with just a few (typical α-capture) elemental abundances were excluded from this work, as they cannot sufficiently constrain supernova models. We further excluded stars where there was ambiguity in the stellar parameters (and therefore the chemistry), usually where a star is equally likely to be a dwarf or subgiant.

3 MASS AND IMF FITTING

With the assembled chemical abundances for all metal-poor stars, we used the STARFIT[2] code to infer progenitor masses, remnant masses, and explosion energies. STARFIT will efficiently find the best-fitting model to an observed chemical abundance pattern by comparison to a large data base of nucleosynthesis yields and their associated progenitor properties. The assumption is made that the observational uncertainties are normally distributed in logarithmic space and that the abundance values are uncorrelated. This allows the reduced χ^2 residual to be used as a measure of the quality of fit of a model to observations. The residual is defined as

$$\tilde{\chi}^2 = \frac{1}{N}\sum_{i=1}^{N}\begin{cases}\left(\frac{o_i - a_i}{\sigma_i}\right)^2 & \text{if } o_i \text{ is a detection}\\ -2\ln\Phi\left(-\frac{o_i - a_i}{\sigma_i}\right) & \text{if } o_i \text{ is an upper limit}\end{cases} \quad (1)$$

where N is the number of elements being matched, o_i is the observed abundance of element i in dex, a_i is the model abundance, σ_i is the uncertainty in the observation, and Φ is the Cumulative Distribution Function of the normal distribution. Elements for which the model yields are lower than an observational upper limit do not, in principle, contribute to the residual. There exists, however, an uncertainty on the value of the upper limit, which is also assumed to be normally distributed, and thus the contribution to the residual is integrated over the distribution of the upper limit. For each model in the data base, the optimal dilution ratio (i.e. the one that minimizes the residual) with pristine big bang material is calculated by means of Newton-Raphson iteration. Since we only consider contributions from individual yields, the yield with the lowest residual after dilution is chosen as the best fit.

We used both the supernova models of Heger & Woosley (2010) and the pair-instability models of Heger & Woosley (2002), and excluded Li abundances as they vary substantially throughout a star's lifetime. Similarly, due to CNO cycling, we opted to fit the sum of C, N, and O abundances simultaneously wherever possible rather than the individual abundances. As recommended by Heger & Woosley (2010), Sc and Cu were treated as model lower limits because they have multiple different nucleosynthetic pathways. We opted to exclude elemental abundances past the iron peak ($Z > 30$) as the nucleosynthetic origin of these elements in Population III stars is quite uncertain. Each STARFIT fit provides an explosion energy, a

[1] Described in Suda et al. (2008, 2011) and Yamada et al. (2013) and available at http://saga.sci.hokudai.ac.jp/wiki/doku.php. The data were retrieved on 2015 August 7.

[2] Available through http://www.starfit.org.

Table 1. Metal-poor star abundances used in this study.

Star	α (J2000) [hms]	δ (J2000) [hms]	$T_{\rm eff}$ [K]	log g	[Fe/H]	ξ [km s^{-1}]	Source
BD+44 493	02:26:49.7	+44:57:46	5430	3.4	−3.8	1.3	Ito et al. (2013)
BS 16076−006	12:48:22.7	+20:56:44	5199	3.0	−3.81	1.4	Bonifacio et al. (2009)
BS 16467−062	13:42:00.6	+17:48:40	5388	3.04	−3.7	1.7	Lai et al. (2008)
BS 16550−087	14:10:26.7	+18:01:23	4750	1.31	−3.5	2.3	Lai et al. (2008)
CD−24 17504	23:07:20.1	−23:52:34	5821	3.5	−3.66	1.22	Ishigaki, Chiba & Aoki (2010)
CS 22891−200	20:19:22.0	−61:30:15	4500	0.45	−3.92	2.6	Hollek et al. (2011)
CS 30336−049	20:45:23.5	−28:42:35	4725	1.19	−4.1	2.1	Yong et al. (2013)
S 29498−043	21:00:51.3	−29:54:46	4400	0.6	−3.75	2.3	Aoki et al. (2002)
G 77−61	03:32:38.0	+01:58:00	4000	5.05	−4.03	0.1	Plez & Cohen (2005)
G 238−30	13:17:40.2	+64:15:12	5299	3.39	−3.72	1.19	Ishigaki et al. (2010)
HE 0013−0257	00:16:04.2	−02:41:06	4500	0.5	−3.82	2.1	Hollek et al. (2011)
HE 0048−6408	00:50:45.3	−63:51:50	4378	0.15	−3.75	2.85	Placco et al. (2014)
HE 0049−3948	00:52:13.4	−39:32:36	6466	3.78	−3.68	0.8	Yong et al. (2013)
HE 0057−5959	00:59:54.0	−59:43:29	5257	2.65	−4.08	1.5	Yong et al. (2013)
HE 0107−5240	01:09:29.1	−52:24:34	5100	2.2	−5.3	...	Christlieb et al. (2002)
HE 0132−2429	01:34:58.8	−24:24:18	5294	...	−3.55	...	Cohen et al. (2013)
HE 0134−1519	01:37:05.4	−15:04:24	5500	3.2	−4.0	1.5	Hansen et al. (2014)
HE 0218−2738	02:21:04.0	−27:24:40	6550	4.3	−3.54	0.84	Carretta et al. (2002)
HE 0233−0343	02:36:29.7	−03:30:06	6100	3.4	−4.7	2.0	Hansen et al. (2014)
HE 0302−3417	03:04:28.6	−34:06:06	4400	0.2	−3.7	2.0	Hollek et al. (2011)
HE 0313−3640	03:15:01.8	−36:29:54	6350	3.8	−3.63	1.2	Cohen et al. (2013)
HE 0926−0546	09:29:27.9	−05:59:43	5159	2.50	−3.73	1.8	Cohen et al. (2013)
HE 1012−1540	10:14:53.5	−15:55:54	5520	4.70	−3.51	1.1	Cohen et al. (2013)
HE 1116−0634	11:18:35.8	−06:50:46	4400	0.1	−3.73	2.4	Hollek et al. (2011)
HE 1300+0157	13:02:56.3	+01:41:51	5550	3.30	−3.49	1.3	Cohen et al. (2013)
HE 1310−0536	13:13:31.2	−05:52:13	5000	1.9	−4.2	2.2	Hansen et al. (2014)
HE 1320−2952	13:22:54.9	−30:08:05	5106	2.26	−3.69	1.5	Yong et al. (2013)
HE 1327−2326	13:30:06.0	−23:41:51	6180	2.2	−5.3	...	Frebel et al. (2005)
HE 1337+0012	13:40:02.4	−00:02:18	6070	3.58	−3.52	1.46	Ishigaki et al. (2010)
HE 1357−0123	14:00:01.1	−01:38:08	4600	1.05	−3.8	2.1	Cohen et al. (2013)
HE 1506−0113	15:09:14.3	−01:24:56	5016	2.01	−3.54	1.6	Yong et al. (2013)
HE 2032−5633	20:36:24.9	−56:23:05	6457	3.78	−3.63	1.8	Yong et al. (2013)
HE 2139−5432	21:42:42.4	−54:18:42	5416	3.04	−4.02	0.8	Yong et al. (2013)
HE 2209−3909	22:12:00.7	−38:55:02	6305	4.3	−3.66	1.2	Cohen et al. (2013)
HE 2233−4724	22:35:59.2	−47:08:36	4360	0.4	−3.65	3.0	Placco et al. (2014)
HE 2239−5019	22:42:26.9	−50:04:01	6100	3.5	−4.2	1.8	Hansen et al. (2014)
HE 2302−2154	23:05:25.2	−21:38:07	4675	0.9	−3.9	2.0	Hollek et al. (2011)
HE 2318−1621	23:21:21.5	−16:05:06	4846	1.4	−3.67	1.75	Placco et al. (2014)
SDSS J090733.30+024608.0	09:07:33.3	+02:46:08	5934	4.0	−3.52	1.8	Caffau et al. (2011a)
SDSS J102915.15+172928.0	10:29:15.2	+17:29:28	5811	4.0	−4.99	1.5	Caffau et al. (2011b)
SDSS J103556.10+064143.0	10:35:56.1	+06:41:43	6262	4.0	<-5.07	1.5	Bonifacio et al. (2015)
SDSS J1204+1201	∼12:04	∼+12:01	5467	3.2	−4.34	1.5	Placco et al. (2015)
SDSS J131326.90+001941.0	13:13:26.9	−00:19:41	5200	2.6	−5.0	1.8	Frebel et al. (2015)
SDSS J174259.70+253135.0	17:42:59.7	+25:31:35	6345	4.0	−4.8	1.5	Bonifacio et al. (2015)
SDSS J220924.70−002859.0	22:09:24.7	−00:28:59	6440	4.0	−4.0	1.3	Spite et al. (2013)
SDSS J235718.91−005247.8	23:57:18.9	−00:52:47	5000	4.8	−3.52	0.0	Aoki et al. (2010)
SMSS J004037.56−515025.2	00:40:37.5	−51:50:25	4468	1.05	−3.67	2.45	Jacobson et al. (2015)
SMSS J005953.98−594329.9	00:59:53.9	−59:43:29	5413	3.41	−3.78	1.4	Jacobson et al. (2015)
SMSS J010651.91−524410.5	01:06:51.9	−52:44:10	4486	1.15	−3.63	2.6	Jacobson et al. (2015)
SMSS J022423.27−573705.1	02:24:23.2	−57:37:05	4846	2.33	−3.74	2.05	Jacobson et al. (2015)
SMSS J031300.36−670839.3	03:13:00.3	−67:08:39	5125	2.3	<-7.52	2.0	Bessell et al. (2015)
SMSS J184226.25−272602.7	18:42:26.2	−27:26:02	4450	1.25	−3.73	2.85	Jacobson et al. (2015)

progenitor mass, a remnant mass, strength of mixing during the SN explosion, and a best-fitting residual.

To quantify the uncertainty in derived progenitor masses, we perturbed the measured abundances for each star using their quoted uncertainties and queried STARFIT using the perturbed abundances. We adopted a conservative uncertainty of 0.2 dex for abundances without reported uncertainties. Measurements were assumed to be normally distributed, and upper limits were perturbed by drawing values from a uniform distribution between [X/H] $\sim \mathcal{U}(-8, L)$, where L is the published limit in [X/H] format. We chose to draw from truncated uniform distributions for upper limits as Placco et al. (2015) note low N abundances ([N/H] < -6) are consistently predicted by STARFIT when only upper limits on nitrogen are available. Draws in [X/H] were converted to $\log_\epsilon$(X) before running STARFIT. We repeated this perturbation procedure 30 times for each star. We find four of the stars (HE0048−6408, HE0313−3640,

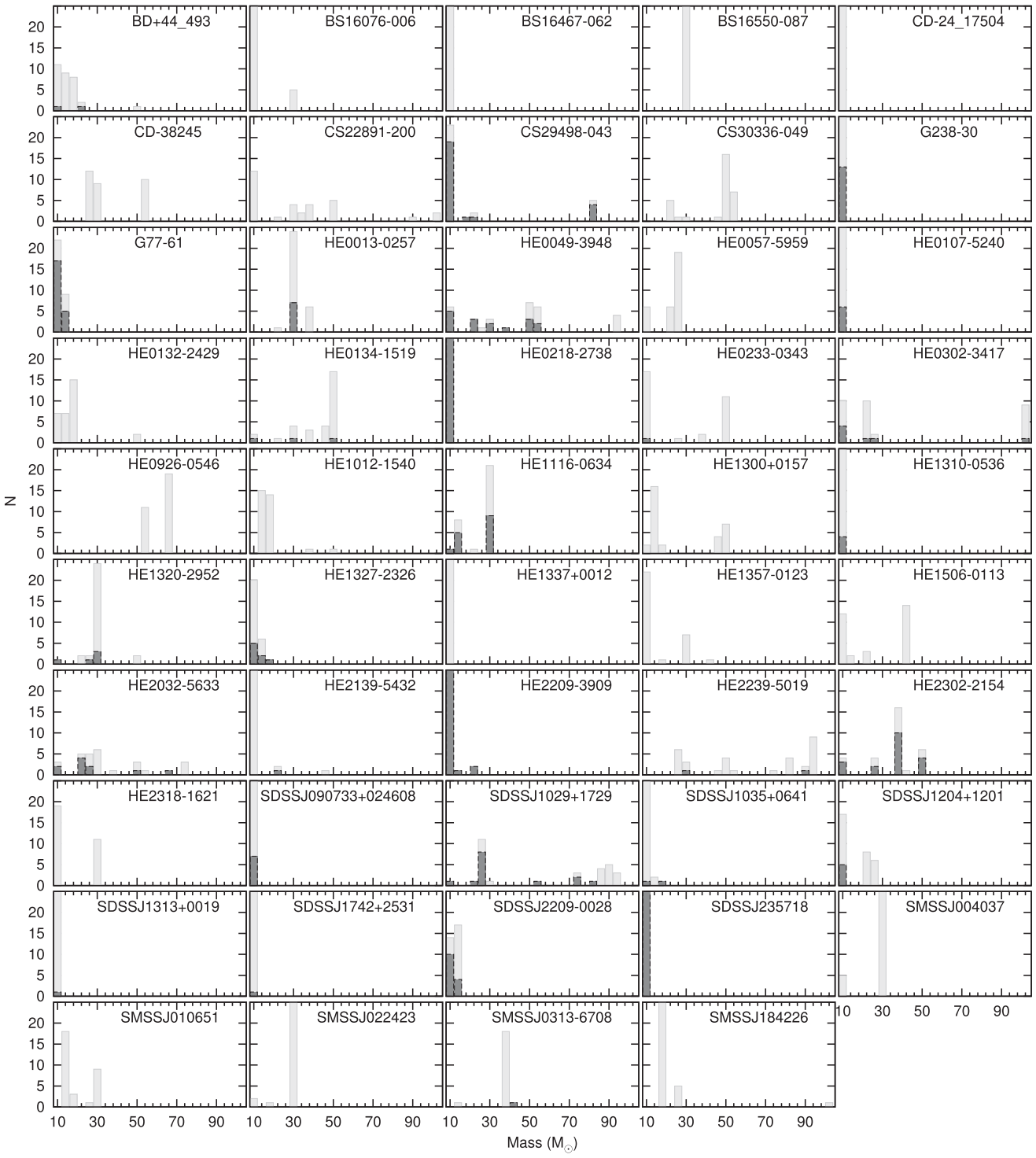

Figure 1. Histograms of derived masses from 30 iterations of STARFIT using perturbed abundances. Light grey bars show fits with a residual of <25, while black lines show fits with a residual of <3.

HE2233−4724, and SMSSJ005953) to have extremely large (>25) best-fitting residuals for all perturbations, and for this reason we discarded these stars from our sample. Numerical noise, uncertain physics (Sukhbold & Woosley 2014), and specifically the grid-like sampling of progenitor masses in supernova models implies that there is a systematic uncertainty floor for a given mass. Our tests demonstrated that a 10 per cent uncertainty in progenitor masses was sufficient to account for this sampling, which we take as representative of the error on the fit. We account for the distribution of recovered progenitor masses by means of a Monte Carlo technique when fitting the IMF. The distribution of inferred progenitor masses for each star, after fitting our perturbed abundance values are shown in Fig. 1. We stress that the error floor does not account for systematic differences between codes. While a detailed investigation of the differing yields from stellar evolution models is beyond the scope of this work, a comparison of solar metallicity models by

Jones et al. (2015) finds generally good agreement among the GENEC, KEPLER, and MESA codes up to the end of core He burning. The differences at latter burning stages, and indeed in explosive nucleosynthesis are harder to assess, and will depend on factors such as where the mass cut is placed when exploding a model, and the degree of fallback after the initial SN collapse. As such, our results should be regarded as model dependant. We note however that for pair-instability SNe, the yields of the models computed by Kozyreva, Yoon & Langer (2014) compare favourably with those of Heger & Woosley (2002).

Sixteen of the stars in our sample also have SN progenitor mass estimates from Placco et al. (2015). Placco et al. use the same STARFIT tool as this work, yet report slightly different progenitor masses than what we find. There are several reasons for these discrepancies. Placco et al. adjust the C abundances based on the evolutionary state of the star, following empirical corrections derived in Placco et al. (2014). If no N measurement is available, the authors also assume [C/N] = 0. In contrast, we opt to fit the combined abundance of C, N, and O. This option is readily available in STARFIT, and implicitly accounts for CNO cycling and the evolutionary state of the star. Differences in abundance choices also contributed to discrepancies in progenitor masses. We employed lower model limits for Cu and Sc (the default recommended option), whereas Placco et al. quote model limits for Cr and Sc. Furthermore, for SMSS J031300.36-670839.3, we opted for the recommended abundances by Bessell et al. (2015), whereas Placco et al. employed the 1D LTE abundances. It also appears that some abundances for elements with $Z < 30$ are not included in the Placco et al. fits. For example, the first star in fig. 8 of Placco et al., SDSS J220924.70−002859.0, is missing both the Na measurement and O upper limit from Spite et al. (2013).

The combination of these discrepancies and analysis choices explains all differences in the inferred progenitor masses; by replicating the Placco et al. STARFIT options, adjusting C and assuming [C/N] = 0, and excluding abundances not present in their fig. 8, we were able to reproduce all of their inferred progenitor masses. It is reassuring to see that even with the systematic differences that arise from using different STARFIT settings, the difference in inferred progenitor masses are reasonably encapsulated by our total uncertainties.

We examined the distribution of derived masses from STARFIT as a function of $T_{\rm eff}$, log g, and [Fe/H]. There is no obvious trend of progenitor mass with stellar parameters, which suggests that our data are not introducing a systematic bias. Encouragingly, we see that of the three stars in our sample with precursor SN masses of $>70 M_{\odot}$, there is a spread in [Fe/H] between −5.0 and −3.6 dex.

We also tested the effects of increasing our metallicity threshold from −3.5 to −3.0 dex. To do this, we took all stars with [Fe/H] between −3.5 and −3.0 dex from Yong et al. (2013), and fitted their abundances as before. We find that the residuals to the fit for the higher metallicity stars are larger. When compared the Heger & Woosley (2002) models, no star above [Fe/H] > 3.0 had a residual <3 (Fig. 2). This can be understood if these stars have been polluted by multiple SNe, and hence cannot be fitted with single SN models. We note that even if we were to include these stars in our initial sample, their large residuals would exclude them from the IMF fit described in the following.

The IMF can be defined as $\xi(M) = AM^{-\alpha}$ where $\xi(M)$ is the probability of finding a star of mass M, the exponent α is the "slope" of the IMF, and A is a normalization constant (Salpeter 1955). To determine the number of stars between masses M_1 and M_2, we simply integrate with respect to M, over the range M_1 to M_2.

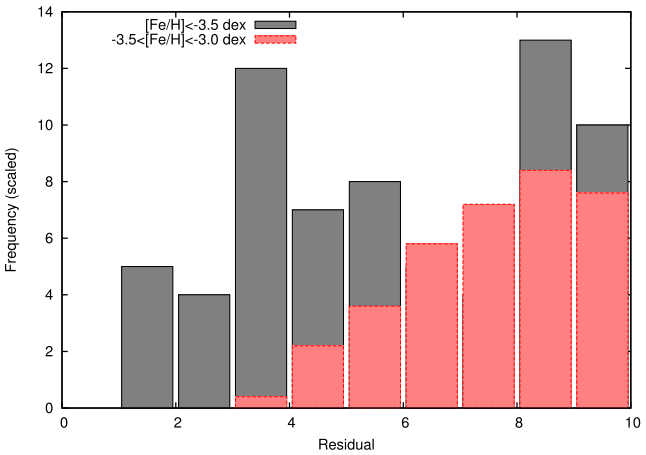

Figure 2. Distribution of residuals to the abundance fits, for stars above and below −3.5 dex. The lack of good fits to the higher metallicity stars is consistent with their being polluted by multiple SNe.

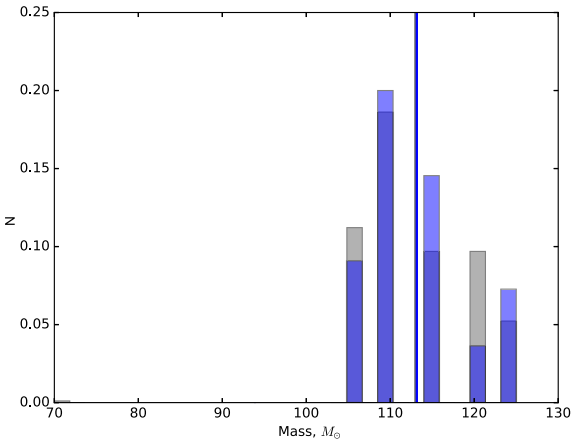

Figure 3. The normalized distribution of masses from 500 sets of perturbed abundances for a single star (grey) compared the distribution from 30 perturbed abundances (blue) and normalized histograms of mass for one star (grey = 500 trials and blue = 30). The thin line marks the mean of each set of trials. Note that no cut has been applied to the fits based on their residuals.

When fitting the observed distribution of Population III supernova progenitor masses to the IMF, we have three free parameters: α, and the minimum and maximum mass for an SN progenitor, $M_{\rm min}$ and $M_{\rm max}$ respectively. As can be seen from Fig. 1, the masses derived for each progenitor when perturbing abundances are not normally distributed. We hence employed a Monte Carlo technique, where we fit the IMF to our observed data 50 000 times. For each iteration, we randomly draw a mass for each star from the 30 perturbed measurements, discarding any masses where STARFIT returned a residual of greater than 3 when fitting abundances. For a single star, we also tested the distribution of masses obtained from 500 perturbed measurements, and encouragingly found this to be compatible with that obtained from 30 (Fig. 3). The parameters of the IMF from each Monte Carlo iteration were simply taken as those values which minimized the χ^2 value of the fit, as shown in Fig. 4. The constraint that the residual of the STARFIT model must be <3 reduces the size of the sample from 49 stars to 29.

Given the progenitor masses in shown in Fig. 1, the best-fitting values (and 16th/84th percentile uncertainties) we infer for the

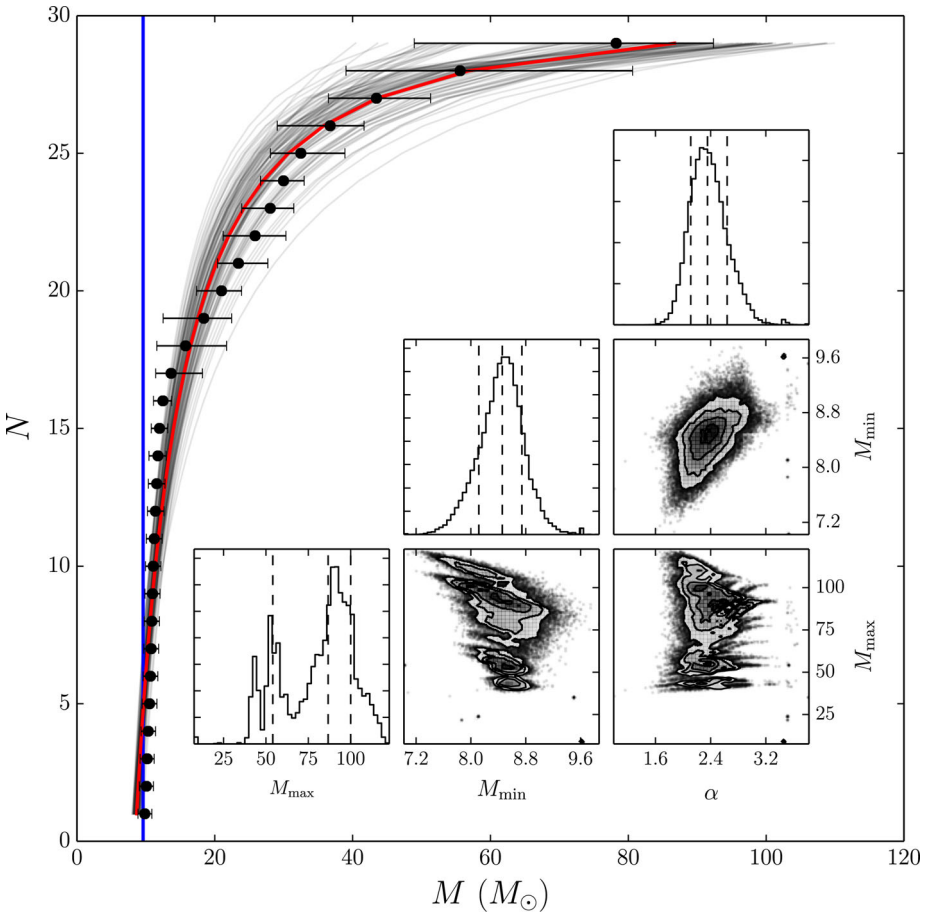

Figure 4. Main panel: the cumulative distribution of Population III supernova progenitor masses to which the IMF was fit. Black points show the mean mass of the nth star across all Monte Carlo iterations. Error bars correspond to the 16th and 84th percentile ranges (i.e. $\simeq 1\sigma$ of the mass of the nth star, added in quadrature with the 10 percent error floor.) The light grey lines show 100 IMFs as fitted during Monte Carlo iterations, while the red line show the final best-fitting IMF. The blue vertical line shows the lower mass limit of 9.6 $M_\odot$ for the model grid used with STARFIT. Inset panel: best-fitting values for α, $M_{\rm min}$, and $M_{\rm max}$ from 50 000 Monte Carlo iterations. The distribution of values for each parameter is shown with a histogram, and the best-fitting value and 16th and 84th percentile limits are marked with dashed lines. $M_{\rm min}$ and $M_{\rm max}$ are in units of $M_\odot$.

IMF are $\alpha = 2.35^{+0.29}_{-0.24}$, a formal minimum SN progenitor mass of $M_{\rm min} = 8.5^{+0.2}_{-0.4} M_\odot$ and a maximum SN progenitor mass of $M_{\rm max} = 87^{+13}_{-33} M_\odot$. Since the minimum mass for Population III supernovae in the data base is $9.6 M_\odot$, however, the conclusion is that the lower IMF endpoint must lie below the minimum mass for Population III supernovae. From the present data, no conclusion can be drawn, however, as to how far below that may be.

4 DISCUSSION AND CONCLUSIONS

Overall, the fit to the inferred Population III supernova progenitor masses found in Section 3 appears quite good. In detail, there are three mass ranges where the quality of the fit appears to vary. Above 30 $M_\odot$ the inferred masses match the fitted IMF extremely well. We find that the distribution of possible maximum masses for a Population III supernova progenitor to be roughly bimodal, with a main peak at $\sim$90 $M_\odot$, and a smaller peak at $\sim$50 $M_\odot$. There is a small tail of Monte Carlo trials which accommodate an upper mass limit to our sample of $\lesssim$120 $M_\odot$, but none above this. We also note that the upper mass limit is relatively insensitive to α.

Between 15 and 30 $M_\odot$, the inferred progenitor mass distribution appears to lie slightly below the best-fitting IMF. The models to which we fit the abundances have masses in steps of at most 0.5 $M_\odot$ over this mass range, so grid effects are unlikely to be the cause of this. An alternative possibility is that an appreciable fraction of stars with zero-age main-sequence masses in the range 15–30 $M_\odot$ massive stars do not explode as SN but make black holes instead (Sukhbold & Woosley 2014), and hence do not eject their synthesized material to enrich subsequent generations of star formation.

Below 15 $M_\odot$ the inferred masses appear to follow a somewhat steeper IMF than our best fit, suggesting that the exponent α may be slightly higher. The IMF is pulled towards shallower slopes (i.e. smaller values of α) by the stars in the 15–30 $M_\odot$ range. If these were excluded, then the fit could better accommodate the lower mass stars, although we are wary of arbitrarily removing stars to improve the fit. The formally deduced minimum mass of $8.5^{+0.2}_{-0.4} M_\odot$ from statistical sampling lies well below the minimum mass for Population III supernovae as reflected by stars in the model data base. We can infer that there is no evidence that the minimum mass for a Population III SN was significantly higher than eight solar masses. However, as the lower mass limit is close to the edge of the model grid at $10 M_\odot$ we stress that we cannot determine from this data whether the IMF for all stars (and not just those that explode) extends to much lower masses.

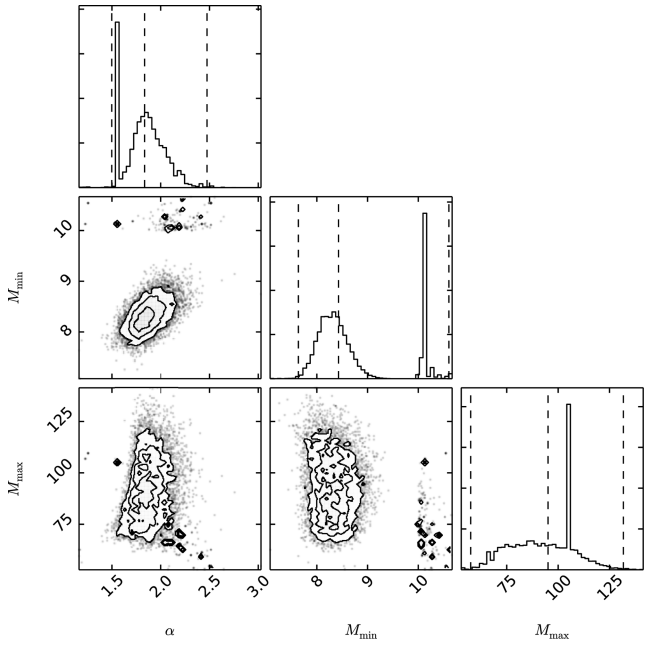

Figure 5. The best-fitting values of α, $M_{\rm min}$, and $M_{\rm max}$ from Monte Carlo trials, fitting the 46 stars which had derived SN progenitor masses with residuals from STARFIT <10. The distribution of values for each parameter is shown with a histogram, and the best-fitting value and 16th and 84th percentile limits are marked with dashed lines. $M_{\rm min}$ and $M_{\rm max}$ are in units of $M_{\odot}$.

As a test, we also relaxed our constraint that the residual of the STARFIT models must be <3, and allowed for models with a residual of up to 10. 46 stars had acceptably fitted masses, and these gave a lower limit of $8.3^{+0.8}_{-0.7}$ $M_{\odot}$, and an upper mass limit of between 70 and 110 $M_{\odot}$ (with no clear peak in the distribution), as shown in Fig. 5. Again, a contribution from stars above 125 $M_{\odot}$ can be excluded at high significance, although interestingly the fit prefers a flatter IMF slope of $\alpha = 1.8^{+0.7}_{-0.3}$ (which is however still formally consistent with the result from stars with residual <3).

We find the best-fitting value of the exponent in the IMF to be 2.35, which is identical to the canonical value of Salpeter (1955), and perhaps suggests that star formation in the metal-free Universe is not so dissimilar to that in the present day. We see no evidence for stars above $\sim$120$M_{\odot}$ exploding in our sample and no signs of the hypothesized pair-instability SNe which may have enriched the Universe at the earliest times. However, we caution that our sample is small, and with 29 stars drawn from a Salpeter IMF between 8 and 300 $M_{\odot}$ we would have only a one in three chance of seeing a star above 150$M_{\odot}$. Hence we cannot set strong limits on the existence of very massive stars which exploded as pair-instability SNe with the current data set. However, increasing the size of our sample of EMP stars will allow for stronger constraints to be placed on Population III SN progenitors in the future.

For comparison, in the present, approximately solar metallicity local Universe, direct detections of core-collapse supernova progenitors in a volume limited sample indicate that most of these are stars have masses $\lesssim$17$M_{\odot}$ (Smartt 2015). Similar conclusions can be drawn from modelling of nucleosynthetic yields of individual SNe (Jerkstrand et al. 2014). This apparent dearth of relatively high-mass SN progenitors in nearby galaxies stands in contrast to what we infer in this Letter for Population III SN progenitors.

We note that the fact that perturbing abundances within their quoted uncertainties affects the inferred progenitor mass to such a large extent (as shown in Fig. 1) demonstrates the necessity of propagation or sampling techniques to account for the full distribution of progenitor masses.

Finally, we emphasize that our abundance probe is only a reflection of the fraction of stars that do explode as SNe; we have no probe of stars that do not explode because they make black holes or are too low mass. Variation in explosion energy, the amount of matter that is enriched by supernovae of a given mass, and the potentially environment-dependent fraction of such gas forming low-mass stars, may also affect the conclusions drawn above and will require further extended studies of first star formation and death.

ACKNOWLEDGEMENTS

We thank the anonymous referee for their helpful and constructive comments. This work was supported by the European Union FP7 programme through ERC grant number 320360. MF is supported by a Royal Society – Science Foundation Ireland University Research Fellowship. AH was supported by Australian Research Council through a Future Fellowship (FT120100363). This research has made use of the SIMBAD data base, operated at CDS, Strasbourg, France, the SAGA data base (Suda et al. 2008), NASA's Astrophysics Data System, the excellent TRIANGLE package (Foreman-Mackey et al. 2014), and Astropy (Astropy Collaboration et al. 2013).

REFERENCES

Aoki W., Norris J. E., Ryan S. G., Beers T. C., Ando H., 2002, ApJ, 576, L141
Aoki W., Beers T. C., Honda S., Carollo D., 2010, ApJ, 723, L201
Astropy Collaboration et al., 2013, A&A, 558, AA33
Bastian N., Covey K. R., Meyer M. R., 2010, ARA&A, 48, 339
Beers T. C., Christlieb N., 2005, ARA&A, 43, 531
Bessell M. S. et al., 2015, ApJ, 806, L16
Bonifacio P. et al., 2009, A&A, 501, 519
Bonifacio P. et al., 2015, A&A, 579, A28
Bromm V., Coppi P. S., Larson R. B., 1999, ApJ, 527, L5
Caffau E. et al., 2011a, A&A, 534, A4
Caffau E. et al., 2011b, Nature, 477, 67
Carretta E., Gratton R., Cohen J. G., Beers T. C., Christlieb N., 2002, AJ, 124, 481
Casey A. R., Schlaufman K. C., 2015, ApJ, 809, 110
Chen K.-J., Bromm V., Heger A., Jeon M., Woosley S. E., 2015, ApJ, 802, 13
Christlieb N. et al., 2002, Nature, 419, 904
Christlieb N., Schörck T., Frebel A., Beers T. C., Wisotzki L., Reimers D., 2008, A&A, 484, 721
Clark P. C., Glover S. C. O., Smith R. J., Greif T. H., Klessen R. S., Bromm V., 2011, Science, 331, 1040
Cohen J. G., Christlieb N., Thompson I., McWilliam A., Shectman S., Reimers D., Wisotzki L., Kirby E., 2013, ApJ, 778, 56
Foreman-Mackey D., Price-Whelan A., Ryan G., Rice E., Smith M., Barbary K., Hogg D. W., Brewer B. J., 2014, Zenodo, 10.5281/zenodo.11020
Frebel A. et al., 2005, Nature, 434, 871
Frebel A., Chiti A., Ji A. P., Jacobson H. R., Placco V. M., 2015, ApJ, 810, L27
Greif T. H., Springel V., White S. D. M., Glover S. C. O., Clark P. C., Smith R. J., Klessen R. S., Bromm V., 2011, ApJ, 737, 75
Hansen T. et al., 2014, ApJ, 787, 162
Heger A., Woosley S. E., 2002, ApJ, 567, 532
Heger A., Woosley S. E., 2010, ApJ, 724, 341

Hollek J. K., Frebel A., Roederer I. U., Sneden C., Shetrone M., Beers T. C., Kang S., Thom C., 2011, ApJ, 742, 54
Ishigaki M., Chiba M., Aoki W., 2010, PASJ, 62, 143
Ito H., Aoki W., Beers T. C., Tominaga N., Honda S., Carollo D., 2013, ApJ, 773, 33
Jacobson H. R. et al., 2015, ApJ, 807, 171
Jerkstrand A., Smartt S. J., Fraser M., Fransson C., Sollerman J., Taddia F., Kotak R., 2014, MNRAS, 439, 3694
Ji A. P., Frebel A., Bromm V., 2015, MNRAS, 454, 659
Jones S., Hirschi R., Pignatari M., Heger A., Georgy C., Nishimura N., Fryer C., Herwig F., 2015, MNRAS, 447, 3115
Kozyreva A., Yoon S.-C., Langer N., 2014, A&A, 566, A146
Lai D. K., Bolte M., Johnson J. A., Lucatello S., Heger A., Woosley S. E., 2008, ApJ, 681, 1524
Norris J. E. et al., 2013, ApJ, 762, 25
O'Shea B. W., McKee C. F., Heger A., Abel T., 2008, in O'Shea B. W. ed., AIP Conf. Ser. Vol. 990, First Stars III, Am. Inst. Phys., New York, 13
Placco V. M., Frebel A., Beers T. C., Christlieb N., Lee Y. S., Kennedy C. R., Rossi S., Santucci R. M., 2014, ApJ, 781, 40
Placco V. M., Frebel A., Lee Y. S., Jacobson H. R., Beers T. C., Pena J. M., Chan C., Heger A., 2015, ApJ, 809, 136
Plez B., Cohen J. G., 2005, A&A, 434, 1117
Salpeter E. E., 1955, ApJ, 121, 161
Schaerer D., 2002, A&A, 382, 28
Schlaufman K. C., Casey A. R., 2014, ApJ, 797, 13
Smartt S. J., 2015, PASA, 32, e016
Sobral D., Matthee J., Darvish B., Schaerer D., Mobasher B., Röttgering H. J. A., Santos S., Hemmati S., 2015, ApJ, 808, 139
Spite M., Caffau E., Bonifacio P., Spite F., Ludwig H.-G., Plez B., Christlieb N., 2013, A&A, 552, A107
Suda T. et al., 2008, PASJ, 60, 1159
Suda T., Yamada S., Katsuta Y., Komiya Y., Ishizuka C., Aoki W., Fujimoto M. Y., 2011, MNRAS, 412, 843
Sukhbold T., Woosley S. E., 2014, ApJ, 783, 10
Tominaga N., Iwamoto N., Nomoto K., 2014, ApJ, 785, 98
Whalen D. J., Fryer C. L., Holz D. E., Heger A., Woosley S. E., Stiavelli M., Even W., Frey L. H., 2013, ApJ, 762, L6
Yamada S., Suda T., Komiya Y., Aoki W., Fujimoto M. Y., 2013, MNRAS, 436, 1362
Yong D. et al., 2013, ApJ, 762, 26

This paper has been typeset from a TEX/LATEX file prepared by the author.